

## Session 2 – B

# Assessing the Influence of Microstructural Features on Deformation of Rocks under Triaxial Loading

Silva<sup>1</sup> SAV, Rathnapriya<sup>1</sup> RHDL, Riyasath MSM.<sup>1</sup>, \*Dassanayake<sup>1</sup> ABN, Fujii.<sup>2</sup> Y  
and Wickrama<sup>1</sup> MADMG

<sup>1</sup>Department of Earth Resources Engineering, University of Moratuwa, Sri Lanka

<sup>2</sup>Sustainable Resources Engineering Division, Hokkaido University, Japan

\*Corresponding author – anjula@uom.lk

## Abstract

Assessing the influence of microstructural features on the deformation of rocks under triaxial loading is vital in rock engineering applications, aiding safe and efficient operations by predicting the deformation of rocks. Triaxial testing offers the simulation of stress conditions within a rock to examine the deformation of rocks with confinements. This research focuses on how microstructural features, such as cementing material and pore geometry, affect the deformation behaviour of rocks subjected to triaxial loading. Two rock types were considered in this study: Kimachi sandstone (medium hard clastic rock) and Bibai sandstone (hard clastic rock). The progressive failure behaviour under Hydro Mechanical (HM) coupling effect was analysed by stress-strain distribution and the fracture geometry was examined using CT images of the specimens which were tested under different confinements. Thin sections were analysed to examine the changes in porosity and the effect on the cementing material with the confinement. The results of the proposed approach reveal a clear influence of the effective confinement on the failure of rocks and how it influences the porosity and cementing material of rocks. It is found that the Bibai sandstone shows a brittle failure and a shearing deformation while Kimachi sandstone shows a brittle to ductile failure and shearing to compaction deformation with the confinement due to the less presence of cementing material within Bibai sandstone compared to Kimachi sandstone. Therefore, with the confinement, the porosity of Bibai sandstone increases while it decreases in Kimachi sandstone. The results highlight the differences in the failure mechanism of a particular rock type for the same effective confinement which is a result of only a partial contribution of the pore pressure on the failure. These findings provide valuable insight into the assessment of microstructural features on the deformation of rocks under triaxial loading, aiding in the development of safer and more efficient rock engineering operations.

*Keywords: CT-images; Deformation; Porosity; Sandstone; Thin section images*

---

## 1. Introduction

In subsurface excavations, existing stress conditions, or insitu stress conditions, are disturbed, and they tend to redistribute around the excavation boundary, creating an Excavation Disturbed Zone (EdZ) and an Excavation Damaged Zone (EDZ). In the EdZ and EDZ, considerable impact is sustained on the instantaneous stability as well as the stability in the long run of the excavation, due to the changes in stresses and permeability, particularly concerning Hydro-Mechanical (HM) processes [1],[2]. Hence, in geomechanics, it is crucial to investigate the influence on rock due to the HM coupling effect. The HM coupling effect on rock is typically examined through laboratory triaxial tests with different confining pressures and pore pressures. In geomechanics applications in rock masses, such as tunneling, mining, the petroleum industry, and radioactive waste disposal, it is crucial to understand how the microstructural characteristics of saturated rock influence the failure mechanism,

specifically the response to the hydro-mechanical coupling effect under triaxial loading conditions.

The failure mechanism of saturated rocks does not depend solely on the stresses in underground conditions but also on their mineral composition and microstructural features such as pores, fissures, and cementing material within the saturated rock mass. Hence, assessing this influence of microstructural characteristics and loading conditions of the saturated rocks on its failure mechanism will fill the gap between fundamental rock mechanics and its real-world applications. Computed Tomography (CT) image analysis provides a great insight into the aforementioned case. Also, digital image analysis and 3D reconstruction of already failed rock specimens are optimal for understanding the microstructural characteristics and evaluating the cracks of the rocks [3]. Software such as ImageJ [4],[5], 3D Slicer and Avizo [6] provide a better platform for analyzing the CT and thin section images.

This research offers a thorough study aimed at the characterization of failure mechanisms in saturated rocks under triaxial loading through combined triaxial testing, thin section image analysis and CT imaging analysis of two rock types. The main objective of the study was to comprehensively assess the influence of microstructural features such as pores, fissures, and cementing material on the deformation of rocks under triaxial loading by analyzing the progressive failure mechanism during triaxial testing and assessing how the presence of certain microstructural features, such as pores fissures and cementing material influences the initiation and propagation of failure in rocks.

## 2. Materials and Methods

This research focuses on two rock types: Kimachi sandstone, a medium hard clastic rock and Bibai sandstone, a hard clastic rock. The physical properties of the rock types are given in Table 1.

Table 1 The physical properties of rock types

Rock Type	Dry Density (g/cm <sup>3</sup> )	Effective Porosity (%)	UCS (Saturated) (MPa)
Kimachi Sandstone	1.98 ± 0.01	18.54 ± 2.0	20.5 ± 2.4
Bibai Sandstone	2.47 ± 0.01	5.59 ± 0.22	101.9 ± 2.3

Rock specimens, 60mm in length and 30mm in diameter were extracted from the rock block in the direction where P-wave velocity was slowest and to achieve a parallelism of 2/100, specimen ends were polished. Thereafter they were saturated in pure water utilizing a water-submersible vacuum jar. Vinyl tapes were used to attach stainless steel endpieces with central holes to the specimens. Subsequently, two cross-type strain gauges were glued to the center of opposite sides of the specimen. A silicon sealant was coated on the specimen to maintain the water flow within the specimen. To avoid contact with confining fluid, a heat-shrinkable tube was equipped to the specimen with attached end pieces. Thereafter it was kept undisturbed in pure water for 24 hours.

Axial load was applied to the specimen using a loading frame and the confining pressure was maintained during the experiment by connecting a double ball plunger pump which comes with a relief valve to the triaxial cell. Water flow holes and pore pressure sensors which come with stainless steel attachments were fixed to the equipped specimen and to control pore pressure, a syringe pump was connected to the lower attachment.

The experiment was started by placing an equipped specimen in the triaxial cell. After the setup was completed, axial stress, confining pressure and pore pressure values were gradually increased till the target values were obtained.

Triaxial testing was done at a strain rate of 10-5 s<sup>-1</sup> (0.036 mm/min.) until axial strain reached 5% in drained conditions at a temperature of 295 K. During the experiment, the measurements of load, stroke, pore pressure and confining pressure were recorded in a data logger regularly at an interval of 1 second.

Table 2 Applied confining and pore pressures during triaxial testing [7]

<b>Confining pressure (MPa)</b>		<b>Pore pressure (MPa)</b>		
2	1			
5	1	4		
10	1	4	9	
15	1	4	9	14

The CT images were obtained in three perpendicular planes with a resolution of 37 μm and thin section images of specimens were prepared for the specimens which were used for triaxial testing under 2 MPa and 15 MPa confining pressures with a pore pressure of 1 MPa, and they were impregnated with blue resin.

### **2.1 Progressive Failure Mechanism using Stress-Strain Distribution**

The failure mechanism of the saturated rocks was studied using the stress-strain distribution of those rocks that had undergone triaxial testing. The stress-strain distributions were plotted and analyzed to determine key mechanical properties exhibited in pre-peak and post-peak regions of complete stress-strain curves such as yield strength, ultimate (peak) strength, residual strength, and strain at failure.

### **2.2 Thin Section Image Analysis**

Blue resin impregnated thin section images were used to identify the microstructural features in rocks subjected to deformation under triaxial conditions, such as pore spaces, fissures, and cementing material, to understand how those microstructural features can influence the failure of saturated rocks under triaxial loading conditions.

The analysis was done using ImageJ which is an open-source software. Initially, the thin section images which are in tiff format were converted into RGB stack images for the pore spaces segmentation and the porosity was obtained. This was done to compare the porosity changes of the provided rock types with confinement after the failure from triaxial testing.

### **2.3 CT Image Analysis**

This was done to reconstruct the fractured saturated rock specimens under triaxial loading conditions in 3D space, to evaluate the fracture geometry and fracture network connectivity. 3D Slicer software was utilized for the above mentioned purpose.

Initially, Image J software was utilized to convert the Disc type Iso-Image files into JPEG format. The preprocessed CT images of the rock specimens which were in JPEG format were added to the 3D Slicer and then the image spacing values were adjusted for all three orthogonal directions. The volume rendering module was utilized to visualize the rock specimens in 3D space.

## **1. Results and Discussion**

### **3.1 Progressive Failure Mechanism using Stress-Strain Distribution**

The results show that the yield strength, peak strength, and residual strength of Bibai sandstone are higher than Kimachi sandstone as illustrated in Figure 1 and that is as expected since Bibai sandstone is a hard clastic rock whereas Kimachi sandstone is a medium hard

clastic rock. The yielding strength, peak strength and residual strength increase with confinement in both rock types (Figure 1) and the reason for that is more stresses can be carried by the material with higher confinements since higher confinements can hold the material together while preventing fissures and cracks getting wider. The failure of Kimachi sandstone has changed from brittle to ductile behavior (Figure 1(a)) and the deformation mode has changed from shearing to compaction with confinement whereas Bibai sandstone showed a brittle failure mode (Figure 1(b)) and shearing deformation mode for all confinements. Since both rock types are sandstones, the differences in failure and deformation modes can be due to the influence of their microstructural features on the deformation.

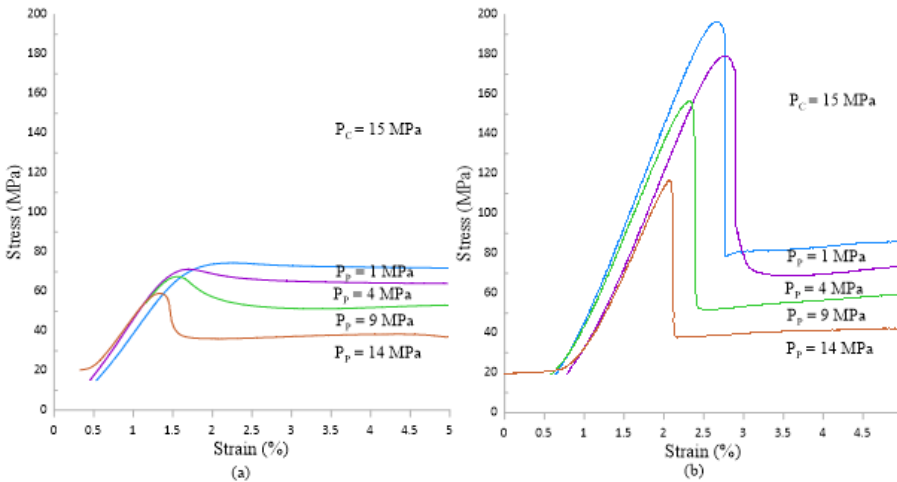


Figure 4 Stress-Strain distributions (a) for Kimachi sandstone (b) for Bibai sandstone

### 3.2 Thin Section Image Analysis

#### 3.2.1 Pore spaces segmentation

The porosity calculation was done for the provided thin sections of both rock types to study the porosity changes with confinement. Results show a slight increment of porosity in Bibai sandstone and a slight decrement of porosity in Kimachi sandstone respectively (Figure 2). Since the Kimachi sandstone showed a shearing to compaction deformation with confinement its porosity can be decreased with confinement as per the results. The deformation was shearing for all confinements in Bibai sandstone and its brittleness increased with confinement resulting in an increment of porosity with confinement.

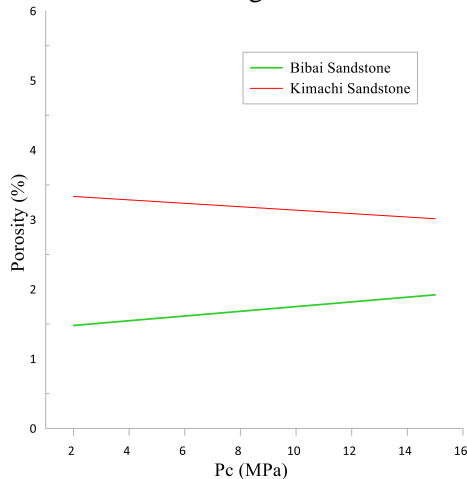
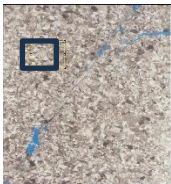

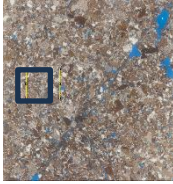
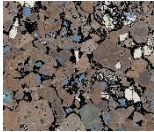

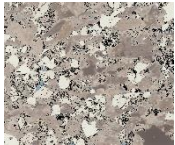
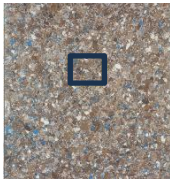
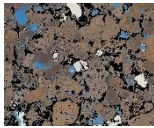


Figure 5 Porosity versus confining pressure plot for both rock types

### 3.2.2 Cementing material segmentation

The results obtained from cementing material segmentation in the selected non-fractured areas of the thin sections are given in Table 3 and by analyzing them qualitatively, it shows that the amount of cementing material presence is higher in Kimachi sandstone than in Bibai sandstone. This could be the reason for brittle failure with confinement in Bibai sandstone unlike Kimachi sandstone which showed a brittle-to-ductile failure with confinement.

Table 3 Segmented cementing material of the chosen areas on thin sections

	Bibai Sandstone		Kimachi Sandstone	
Pc = 2 MPa				
Pc = 15 MPa				

### 3.3 CT Image Analysis

As per the 3D reconstructed rock specimens, Bibai sandstone shows a shearing deformation for all confinement and two shear planes can be seen when the effective confinement is low. Kimachi sandstone shows a shearing to compaction deformation with confinement.

Table 4 Deformation modes of 3D reconstructed rock specimens

Rock Type	Specimen No.	Pc (MPa)	Pp (MPa)	Deformation Mode
Bibai Sandstone	3	15	1	Shearing
	4	15	4	Shearing
	5	15	9	Shearing
	6	15	14	Shearing-two shear planes
Kimachi Sandstone	5	5	1	Shearing
	6	5	4	Shearing
	10	15	1	Compaction
	11	15	4	Shear enhanced compaction

## 2. Conclusion

Based on the results of this study, the yield strength, peak strength, and residual strength of Bibai sandstone are higher than Kimachi sandstone.

Compared to Kimachi sandstone, the presence of cementing material is less in Bibai sandstone, and it shows a brittle failure throughout the increment of confining pressure while Kimachi sandstone shows a brittle-to-ductile failure (Figure 1). The conclusion is that the less presence of cementing material in Bibai sandstone results in a brittle failure with confinement. Therefore, with confinement, brittle failure and increment in brittleness can be seen and the porosity as well as permeability increases. In Kimachi sandstone, the presence of cementing

material is there, resulting in a brittle-to-ductile failure and a reduction in porosity and permeability can be seen with confinement.

The behavior of the failure for the same effective confinement must be similar for the same rock type. Therefore, the strength values of a rock type for the same effective confinement can be expected. However, the results show different strength values (Table 5).

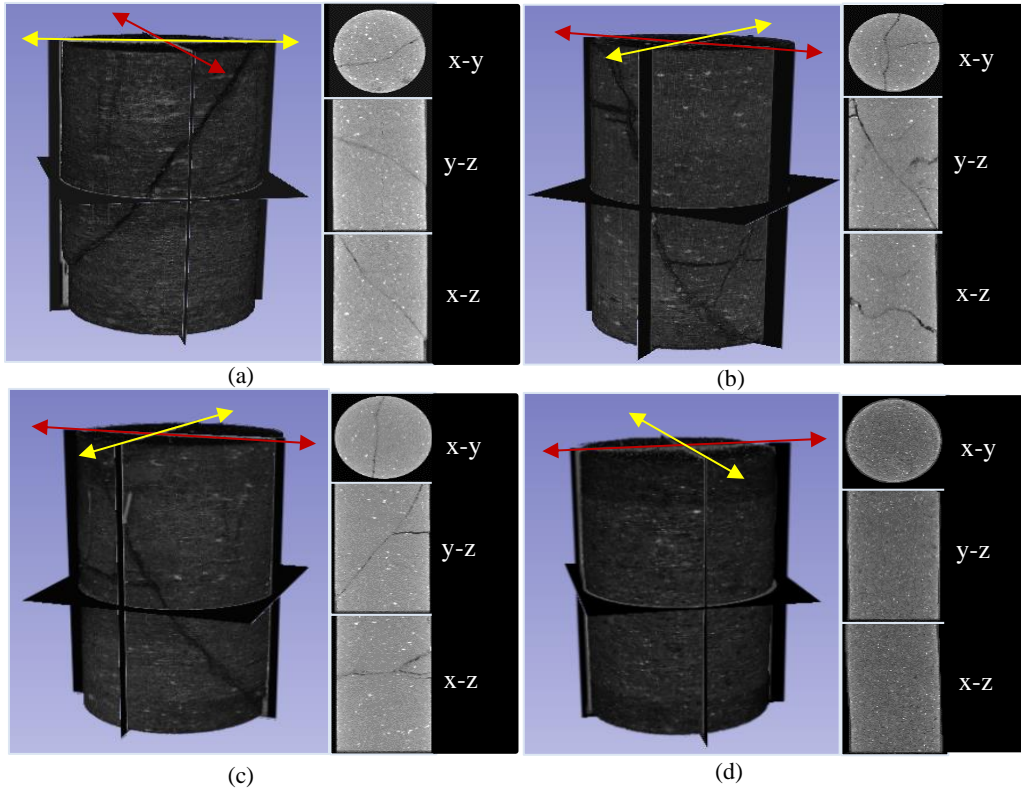


Figure 6 Reconstructed specimens (a),(b) for 3 and 6 specimens of Bibai sandstone respectively (c),(d) for 5 and 10 specimens of Kimachi sandstone respectively

Table 5 Peak strength values

Rock Type	Confining Pressure (MPa)	Pore Pressure (MPa)	Effective Confinement (MPa)	Peak Strength (MPa)
Kimachi Sandstone	2	1	1	38.32
	5	4	1	49.16
	10	9	1	48.78
	15	14	1	59
Bibai Sandstone	2	1	1	92.98
	5	4	1	106.4
	10	9	1	153.24
	15	14	1	156.27

The reason for the above results can be due to the partial contribution of the pore pressure to the failure, where only a fraction of the pore pressure has contributed to the failure.

$$\sigma'_c = \sigma_c - P_p \text{ (Terzaghi's effective stress principle)}$$

$$\sigma'_c = \sigma_c - \alpha \times P_p$$

Where,  $\sigma'_c$ : Effective confining pressure,  $\sigma_c$ : Confining pressure,  $P_p$ : Pore pressure and  $\alpha$ : Fraction of pore pressure which has contributed to the failure.

## References

- [1] J. A. Hudson, O. Stephansson, and J. Andersson, “Guidance on numerical modelling of thermo-hydro-mechanical coupled processes for performance assessment of radioactive waste repositories,” *International Journal of Rock Mechanics and Mining Sciences*, vol. 42, no. 5–6, pp. 850–870, Jul. 2005, doi: <https://doi.org/10.1016/j.ijrmms.2005.03.018>.
- [2] Jonny Rutqvist et al., “Coupled thermal–hydrological–mechanical analyses of the Yucca Mountain Drift Scale Test—Comparison of field measurements to predictions of four different numerical models,” *International Journal of Rock Mechanics and Mining Sciences*, vol. 42, no. 5–6, pp. 680–697, Jul. 2005, doi: <https://doi.org/10.1016/j.ijrmms.2005.03.008>.
- [3] Z. Zhao and X. Zhou, “3D Digital Analysis of Cracking Behaviors of Rocks through 3D Reconstruction Model under Triaxial Compression,” *Journal of Engineering Mechanics- asce*, vol. 146, no. 8, Aug. 2020, doi: [https://doi.org/10.1061/\(asce\)em.1943-7889.0001822](https://doi.org/10.1061/(asce)em.1943-7889.0001822).
- [4] C. A. Schneider, W. S. Rasband, and K. W. Eliceiri, “NIH Image to ImageJ: 25 years of image analysis,” *Nature Methods*, vol. 9, no. 7, pp. 671–675, Jun. 2012, doi: <https://doi.org/10.1038/nmeth.2089>.
- [5] J. Schindelin et al., “Fiji: an open-source Platform for biological-image Analysis,” *Nature Methods*, vol. 9, no. 7, pp. 676–82, 2012, doi: <https://doi.org/10.1038/nmeth.2019>.
- [6] C. Qi, X. Wang, W. Wang, J. Liu, Jincui Tuo, and K. Liu, “Three-dimensional characterization of micro-fractures in shale reservoir rocks,” *Petroleum Research*, vol. 3, no. 3, pp. 259–268, Sep. 2018, doi: <https://doi.org/10.1016/j.ptlrs.2018.08.003>.
- [7] A.B.N. Dassanayake, Y. Fujii, D. Fukuda, and J. Kodama, “A new approach to evaluate effective stress coefficient for strength in Kimachi sandstone,” *Journal of petroleum science & engineering*, vol. 131, pp. 70–79, Jul. 2015, doi: <https://doi.org/10.1016/j.petrol.2015.04.015>.